sintering behavior and microwave dielectric properties of $MgO\text{-}2B_2O_3\text{-}xwt\%H_3BO_3\text{-}ywt\%$BCB ceramics

Haiquan WANG, Shixuan LI, Kangguo WANG, Xiuli CHEN*, Huanfu ZHOU*

Collaborative Innovation Center for Exploration of Hidden Nonferrous Metal Deposits and Development of New Materials in Guangxi, Key Laboratory of Nonferrous Materials and New Processing Technology, Ministry of Education, School of Materials Science and Engineering, Guilin University of Technology, Guilin 541004, China.

Abstract

The bulk density, sintering behavior and microwave dielectric properties of $MgO\text{-}2B_2O_3$ series ceramics synthesized by solid-state reaction method were systematically studied in this paper. X-ray diffraction and microstructural analysis revealed that the as-prepared $MgO\text{-}2B_2O_3$ ceramics possessed a single-phase structure with rod-like morphology. Through the investigation of the effects of different dosages of H_3BO_3 and BCB on bulk density, sintering behavior and microwave dielectric properties of $MgO\text{-}2B_2O_3$ ceramics, the optimum sintering temperature was obtained at an addition of 30*wt*%H_3BO_3 and 8*wt*%BCB and the sintering temperature was reduced to 825 ^oC. The addition of 40*wt* %H_3BO_3 and 4 *wt*%BCB increased the quality factor $Q\times f$, permittivity ε_r and temperature coefficient of resonance frequency τ_f of $MgO\text{-}2B_2O_3$ to 44,306 GHz, 5.1 and -32 ppm/^oC, respectively, meeting the

* Corresponding author, E-mail: cxlnwpu@163.com.

* Corresponding author, E-mail: zhouhuanfu@163.com.

criteria of low-temperature co-fired ceramics.

Keywords: ceramics; $MgO\text{-}2B_2O_3$; H_3BO_3; BCB; Dielectric property

1 Introduction

Due to the low manufacturing cost, short development cycle, and potential for miniaturization and incorporation of electronic devices, low-temperature co-fired ceramics (LTCC) is the trend for electronic components manufacture in the wireless communication and broadcasting industry [1-4]. However, most of the high $Q\times f$ dielectric materials are manufactured at high sintering temperatures. High sintering temperatures not only hinder their incorporation with low melting electrode and polymer based substrates but also lead to huge energy consumption and volatile components evaporation. For practical application, LTCC requires not only excellent microwave dielectric properties but also low sintering temperature and good co-fire matching between ceramics and electrodes [5-10]. Materials with low melting point are often added in order to lower the firing temperatures. However, the microwave dielectric properties were lowered by the addition of low melting point materials.

In the past decades, synthesis of xMgO-$y$$B_2O_3$ ceramic has attracted considerable interest because of its many potential applications in LTCC devices. Davis *et al.* [11] systematically reported the chemistry of $MgO\text{-}B_2O_3$ binary systems, such as $MgO\text{-}B_2O_3$, $MgO\text{-}1/2B_2O_3$ and $MgO\text{-}1/3B_2O_3$. Nishizuka et al. [12] demonstrated that the MgO-$x$$B_2O_3$ (x = 25 and 33) sintered at low temperatures exhibited remarkable dielectric properties with a ε_r of ~7 and $Q\times f$ of 79,100-260,100 GHz (@ x = 33) and 39,600-310,000 GHz (@ x = 25). Zhou *et al.* [13] reported optimal microwave

dielectric properties could be obtained at sintering temperature as low as 1,100°C with a molecular ratio of $MgO:B_2O_3$ = 1:1. The resulted ceramics showed excellent microwave dielectric properties with a ε_r of 5.83, $Q\times f$ of 41,930 GHz and τ_f of ~62 ppm/°C. According to Zhou's work, $MgO\text{-}2B_2O_3$-4wt%$BaCu(B_2O_5)$ ceramics possess good microwave dielectric properties, showing promising potential applications in LTCCs [14].

However, the microwave dielectric properties of B_2O_3-rich ceramics in $MgO\text{-}B_2O_3$ binary system (e.g., $MgO\text{-}2B_2O_3$ and $MgO\text{-}B_2O_3$) have not been investigated in detail. In addition, the sintering temperature of $MgO\text{-}2B_2O_3$ ceramics is still too high for LTCC devices [15]. Sintering additives [16-26], ultrafine powders [27-31], and low sintering temperatures materials [32-34] can be used to reduce the sintering temperature of ceramics. However, the preparation of ultrafine powder with low intrinsic sintering temperatures is expensive, complex and hard to be scaled up. By contrast, the sintering temperature of magnesium oxide was effectively reduced by adding appropriate amount of sintering aid [34] such as B_2O_3, H_3BO_3 and $BaCu(B_2O_5)$ (BCB). However, the microwave dielectric properties of $MgO\text{-}2B_2O_3$-*xwt*%H_3BO_3-*ywt*%BCB ceramics have not been investigated systematically. This is the objective of this research.

2 Experimental procedure

$MgO\text{-}2B_2O_3$-*xwt*%H_3BO_3-*ywt*%BCB ceramics were prepared by solid-state reaction method. MgO (≥98.5%), H_3BO_3(≥ 99%), $Ba(HO)_2\cdot 8H_2O$(≥99%) and CuO (≥99%) were obtained from Guo-Yao Co., Ltd, Shanghai, China. MgO powders were

pre-calcined at 800 ºC for 2 h. The raw materials were weighed according to the molar ratio of MgO:B_2O_3=1:2. The powders were mixed thoroughly in a nylon jar before ball milled for 4 hours. Then, the dried powder mixture was calcined at 800 ºC for 4 h. H_3BO_3 and BCB with different mass ratio were added to the calcined powder. The mixture of H_3BO_3, BCB and calcined powder was re-milled for 4 h and pressed into the form of cylinder with a diameter of 10 mm and height of 4-5 mm under a uniaxial pressure of 100 MPa. Subsequently, the samples were sintered for 4 hours at 750-975 ºC under air.

Archimedes' principle was employed to measure the bulk density. X-ray diffractometer (X'PERT PRO, PANalytical, Almelo, Netherlands) equipped with Cu K_α radiations was used for structural analysis. Scanning electron microscopy (JSM-6380LV, JEOL, Tokyo, Japan) was used to observe the microstructure of as-fired surfaces. A 300 KHz to 20 GHz Network Analyzer (E5071C, Agilent Co., CA, USA) was used to measure the microwave dielectric properties. The τ_f values were calculated in the temperature range of 25 °C to 85 °C, as given below:

$$\tau_{\mathrm{f}} = \frac{f_T - f_{T0}}{f_{T0}(T - T_0)} \times 10^6$$

Where, f_T and f_{T0} represent the resonant frequencies at 85°C (T) and 25 °C (T_0), respectively.

3 Results and discussion

Figure 1 shows the XRD profiles of MgO-2B_2O_3-10*wt*%H_3BO_3-*ywt*%BCB (*y* = 2, 4, 6 and 8) ceramics sintered at their optimal temperatures. The XRD patterns was

indexed as MgB_4O_7 (JCPDS card number 00-031-0787), indicating that the addition of H_3BO_3 and BCB had no effect on the phase structure of ceramics.

SEM images of the MgO-$2B_2O_3$-10*wt*%H_3BO_3-*ywt*%BCB (y = 2, 4, 6, and 8) ceramics sintered at optimal temperatures are shown in Figure 2(a-d). It can be seen that the MgO-$2B_2O_3$ crystals possessed a rod-like shape and refined with the increase of BCB content. As the BCB content increased to 8 *wt* %, the MgO-$2B_2O_3$ crystals exhibited a glassy phase. Moreover, the porosity increased with the increase of BCB content.

Bulk density, ε_r, $Q\times f$, and τ_f of the MgO-$2B_2O_3$-10*wt*%H_3BO_3-*ywt*%BCB (y = 2, 4, 6 and 8) ceramics sintered at different temperatures are shown in Figure 3. It can be seen that the bulk density initially increased with the increase of sintering temperature except for the sample with 2 wt% BCB which showed a slight decrease as shown in Figure 3 (d). The bulk density change is consistent with the appearance of porosity shown in Figure 2(a)-(d).

When sintering temperature increased from 900 °C to 950 °C, the $Q\times f$ of the MgO-$2B_2O_3$-10*wt*%H_3BO_3-2*wt*%BCB ceramics increased from 25,408 GHz to 33,951 GHz, indicating the change of porosity with the sintering temperature change. The minimum porosity was obtained at 900 °C. However, with further increase of sintering temperature, the $Q\times f$ of MgO-$2B_2O_3$-10*wt*%H_3BO_3-2*wt*%BCB ceramics decreased to 32,541 GHz due to over-firing. The $Q\times f$ of MgO-$2B_2O_3$-10*wt*%H_3BO_3-*ywt*%BCB (y = 2, 4, 6 and 8) ceramics first increased and then decreased with the increase of sintering temperatures. The optimum sintering

temperature decreased from 950 °C to 850 °C when BCB content increased from 2 wt% to 8 wt%. The $Q\times f$ reached a maximum of 40,076 GHz when BCB content was 4 wt%, indicating the addition of appropriate amount of BCB reduced the sintering temperature and improved the $Q\times f$ of MgO-2B_2O_3-10*wt*%H_3BO_3 ceramics.

Figure 3(b) shows the ε_r change of MgO-2B_2O_3-10*wt*%H_3BO_3-*ywt*%BCB (y = 2, 4, 6 and 8) ceramics at different temperatures. With the increase of sintering temperature, ε_r increased for ceramics with 6 wt % and 8 wt % BCB but decreased for ceramics with 2 wt % and 4 wt % BCB, indicating the addition of BCB had a significant effect on the ε_r of MgO-2B_2O_3 ceramics.

Figure 3(c) presents the τ_f at different sintering temperatures, which exhibits a similar trend to $Q\times f$. The τ_f of MgO-2B_2O_3-10*wt*%H_3BO_3-2*wt*%BCB ceramic was -40 ppm/°C when the sintering temperature was 925 °C. Then, the τ_f value initially increased with the increase of sintering temperature followed by a slight decrease. The τ_f is affected by the chemical additives and the composition of the ceramic [34, 35]. One should note that the τ_f of MgO-2B_2O_3-10*wt*%H_3BO_3-*ywt*%BCB ceramics demonstrated an overall decreasing trend with the increase of BCB content. Meanwhile, sintering temperature decreased with the increase of BCB content, demonstrating its positive effect as a sintering aid. The best ceramics properties with bulk density of 2.409 g/cm^3, $Q\times f$ of 40,076 GHz, and ε_r of -40 ppm/°C were obtained at 4 *wt* % BCB content and 925 °C.

Figure 4 presents the room-temperature XRD profiles of the MgO-2B_2O_3-*xwt*%H_3BO_3-4*wt*%BCB ($10 \leq x \leq 40$) ceramics sintered at their optimum

temperatures. XRD results showed that the MgO-2B_2O_3-*x*wt%H_3BO_3-4*wt*%BCB ($10 \leq x \leq 40$) ceramics were crystallized in orthorhombic space group Pbca without impurity phases, indicating the addition of H_3BO_3 had no negative affect on the phase structure of ceramics.

Figure 5 shows the SEM images of MgO-2B_2O_3-*x*wt%H_3BO_3-4*wt*%BCB ($10 \leq x \leq 40$) ceramics sintered at their optimum temperatures. Distinctly different microstructure was observed for the ceramics with different H_3BO_3 content. With the increase of H_3BO_3 content, the MgO-2B_2O_3-*x*wt%H_3BO_3-4*wt*%BCB ceramics achieved denser and more homogeneous microstructure. However, at a H_3BO_3 content of 40 wt%, a slight over-burning was observed due to the presence of excessive sintering aid, resulting in abnormal grain growth as shown in Figure 5(d) .

Figure 6 shows the bulk density, ε_r, $Q \times f$ and τ_f of the MgO-2B_2O_3-*x*wt%H_3BO_3-4*wt*%BCB ceramics at different sintering temperatures. The bulk density of ceramics increased initially and then decreased slightly with the increase of H_3BO_3 content except for the ceramics with 10% H_3BO_3. The maximum bulk density of MgO-2B_2O_3-*x*wt%H_3BO_3-4*wt*%BCB with 10% H3BO3 was obtained at sintering temperature of 925 ^oC. However, when H_3BO_3 increased to 20%~40%, the maximum bulk density was obtained at 900 ^oC, indicating the addition of H_3BO_3 as a sintering aid reduced the sintering temperature of ceramics.

In general, the $Q \times f$ of microwave dielectric ceramics is related to the grain size, porosity, densification and secondary phases [36-38]. The $Q \times f$ of MgO-2B_2O_3-*x*wt%H_3BO_3-4*wt*%BCB ceramics increased with the increase of

sintering temperature up to 900 °C and then decreased, showing excellent consistency with the variation of the bulk density. Due to the fact that there was no any secondary phase in MgO-2B_2O_3-*x*wt%H_3BO_3-4wt%BCB ceramics, the $Q \times f$ was mainly affected by sintering temperature and H_3BO_3 content, which altered the density and grain size. At a sintering temperature of 850 °C, MgO-2B_2O_3-10wt%H_3BO_3-4wt%BCB ceramics showed a significant proportion of pores between grains, resulting in a lower $Q \times f$. When sintering temperature was 900 °C, denser microstructure of MgO-2B_2O_3-40wt%H_3BO_3-4wt%BCB resulted in a maximum $Q \times f$ of 44,306 GHz, a relative ε_r of 5.1 and τ_f of -32 ppm/^{o}C.

The dielectric properties depend on relative density, crystal structure, and other phase content [39, 40]. The relative ε_r of MgO-2B_2O_3-*x*wt%H_3BO_3-4wt%BCB ceramics was consistent with the change in bulk density. The maximum ε_r was found to be 4.81 at a H_3BO_3 content of 10 wt%. Also, an overall increase in relative ε_r was observed for H_3BO_3-containing ceramics when H_3BO_3 content increased to 20 wt%, 30 wt% and 40 wt%. Hence, the ε_r was influenced by the variation of H_3BO_3 content, sintering temperature and bulk density.

It is worth emphasizing that the variations of ρ, ε_r, $Q \times f$ and τ_f values for MgO-2B_2O_3-*x*wt%H_3BO_3-4wt%BCB (x = 10, 20, 30 and 40) are consistent with the change of H_3BO_3 content. The optimum sintering temperature of MgO-2B_2O_3-*x*wt%H_3BO_3-4wt%BCB ceramics decreased from 925 °C to 900 °C, the $Q \times f$ increased from 40,076 GHz to 44,306 GHz, the relative ε_r increased from 4.81 to 5.11, the τ_f increased from -40 ppm/^{o}C to -32 ppm/^{o}C, and the bulk density increased

from 2.460 g/cm^3 to 2.463 g/cm^3. The increase of H_3BO_3 content not only lowered the sintering temperature but also improved the microwave dielectric properties of MgO-2B_2O_3-*x*wt%H_3BO_3-4*w*t%BCB ceramics.

Table 1 tabulates the sintering temperatures and microwave dielectric properties of MgO-2B_2O_3-*x*wt%H_2BO_3-*y*wt%BCB ceramics at different BCB and H_3BO_3 content. When the BCB content was fixed, the decrease in sintering temperature was less noticeable with the increase of H_3BO_3 content. The τ_f remained stable at around -32 to -62 ppm/^{o}C. When H_3BO_3 content was constant, the increase of BCB content gradually decreased the sintering temperature. The quality factor increased initially and then decreased at higher BCB content. In summary, the addition of BCB and H_3BO_3 reduced the sintering temperature and increased the quality factor of MgO-2B_2O_3-*x*wt%H_3BO_3-*y*wt%BCB ceramics, which was ascribed to the growth of MgO-2B_2O_3 grains. The optimum sintering temperature of the produced ceramics reduced to 825 °C, indicating that it can be used as an alternative material for LTCC devices.

4 Conclusions

In summary, MgO-2B_2O_3-*x*wt%H_2BO_3-*y*wt%BCB (x = 10, 20, 30, and 40; y = 2, 4, 6, and 8) ceramics were prepared by solid-state method and the influence of H_3BO_3 and BCB contents on the bulk density, sintering behavior and microwave dielectric properties were systematically investigated. MgO-2B_2O_3-10*w*t%H_3BO_3-*y*wt%BCB (y = 2, 4, 6, and 8) ceramics consisted of a single-phase MgO-2B_2O_3 with orthorhombic space group Pbca. The quality factor $Q\times f$ of

$MgO\text{-}2B_2O_3\text{-}10wt\%H_3BO_3\text{-}ywt\%BCB$ (y = 2, 4, 6 and 8) ceramics increased initially and then decreased slightly with the increase of BCB content. The optimal properties of resulted $MgO\text{-}2B_2O_3\text{-}10wt\%H_3BO_3\text{-}4wt\%BCB$ ceramic was ρ= 2.409 g/cm^3, $Q\times f$ = 40,076 GHz, ε_r = 5 and τ_f = - 45 ppm/^{o}C. In addition, the microwave dielectric properties and sintering temperature of $MgO\text{-}2B_2O_3\text{-}xwt\%H_3BO_3\text{-}4wt\%BCB$ ceramics (x = 10, 20, 30, and 40) were improved with the increase of H_3BO_3 content at 4 *wt*% BCB. The resulted $MgO\text{-}2B_2O_3\text{-}40wt\%H_3BO_3\text{-}4wt\%BCB$ showed excellent microwave dielectric properties of 5.1, quality factor of 44,306 GHz and τ_f of -32 ppm/^{o}C. The current work presented a novel approach to modify the τ_f of $MgO\text{-}B_2O_3$ ceramics, which is highly desirable for microwave equipment and devices.

Acknowledgments

This work was supported by Natural Science Foundation of China (Nos. 61761015 and12064007), Natural Science Foundation of Guangxi (Nos. 2018GXNSFFA050001 , 2017GXNSFDA198027 and 2017GXNSFFA198011), High Level Innovation Team and Outstanding Scholar Program of Guangxi Institutes.

References

[1] Sebastian MT, Jantunen H. Low loss dielectric materials for LTCC applications: a review. *Int Mater Rev* 2008**,** ceramics; $MgO-2B_2O_3$; H_3BO_3; BCB; Dielectric property **53**: 57-90.

[2] Zhou HF, Liu XB, Chen XL, et al. $ZnLi_{2/3}Ti_{4/3}O_4$: A new low loss spinel microwave dielectric ceramic. *J Eur Ceram Soc* 2012**, 32**: 261-265.

[3] Zhou D, Guo D, Li WB, *et al*. Novel temperature stable high-epsilon(r) microwave dielectrics in the Bi_2O_3-TiO_2-V_2O_5 system. *J Mater Chem C* 2016**, 4**: 5357-5362.

[4] Zhou D, Pang LX, Wang DW, *et al*. Novel water-assisting low firing MoO_3 microwave dielectric ceramics. *J Eur Ceram Soc* 2019**, 39**: 2374-2378.

[5] Dou G, Zhou DX, Guo M, *et al*. Low-temperature sintered Zn_2SiO_4-$CaTiO_3$ ceramics with near-zero temperature coefficient of resonant frequency. *J Alloys Compd* 2012**, 513**: 466-473.

[6] Wang KG, Zhou HF, Liu XB, *et al*. A lithium aluminium borate composite microwave dielectric ceramic with low permittivity, near-zero shrinkage, and low sintering temperature. *J Eur Ceram Soc* 2019**, 39**: 1122-1126.

[7] Hughes H, Iddles DM, Reaney IM. Niobate-based microwave dielectrics suitable for third generation mobile phone base stations. *Appl Phys Lett* 2001**, 79**: 2952-2954.

[8] Li YX, Li H, Tang B, *et al*. Microwave dielectric properties of low-fired $Li_2ZnTi_3O_8$-TiO_2 composite ceramics with Li_2WO_4 addition. *J Mater Sci - Mater Electron* 2015**, 26**: 1181-1185.

[9] Hao SZ, Zhou D, Hussain F, *et al*. Structure, spectral analysis and microwave dielectric properties of novel $x(NaBi)_{0.5}MoO_4$-$(1-x)Bi_{2/3}MoO_4$ (x=0.2 similar to 0.8) ceramics with low sintering temperatures. *J Eur Ceram Soc* 2020**, 40**: 3569-3576.

[10] Bi JX, Xing CF, Yang CH, *et al*. Phase composition, microstructure and microwave dielectric properties of rock salt structured Li_2ZrO_3-MgO ceramics. *J Eur Ceram Soc* 2018**, 38**: 3840-3846.

[11] Davis H M KMA. The system magnesium oxide-moric oxide. *J Am Ceram Soc* 1945**, 28**: 97-102.

[12] Nishizuka M, Ogawa H, Kan A, *et al.* Synthesis and microwave dielectric properties of MgO-$x$mol%B_2O_3 (x=33 and 25) ceramics in MgO-B_2O_3 system. *Ferroelectrics* 2009**, 388**: 101-108.

[13] Fan GC, Zhou HF, Chen XL. Optimized sintering temperature and enhanced microwave dielectric performance of $Mg_2B_2O_5$ ceramic. *J Mater Sci - Mater Electron* 2017**, 28**: 818-822.

[14] Zhou HF, Tan XH, Liu XB, *et al.* Low permittivity MgO-xB_2O_3-yBaCu(B_2O_5) microwave dielectric ceramics for low temperature co-fired ceramics technology. *J Mater Sci - Mater Electron* 2018**, 29**: 18486-18492.

[15] Zhou HF, Tan XH, Wang KG, *et al.* Microstructure and sintering behavior of low temperature cofired $Li_{4/5}Mg_{4/5}Ti_{7/5}O_4$ ceramics containing BaCu(B_2O_5) and TiO_2 and their compatibility with a silver electrode. *RSC Adv* 2017**, 7**: 44706-44711.

[16] Guo H-H, Zhou D, Du C, *et al*. Temperature stable $Li_2Ti_{0.75}(Mg_{1/3}Nb_{2/3})_{0.25}O_3$-based microwave dielectric ceramics with low sintering temperature and ultra-low dielectric loss for dielectric resonator antenna applications. *J Mater Chem C* 2020**, 8**: 4690-4700.
[17] Iddles DM, Bell AJ, Moulson AJ. Relationships between dopants, microstructure and the microwave dielectric properties of ZrO_2-TiO_2-SnO_2 ceramics. *J Mater Sci* 1992**, 27**: 6303-6310.
[18] Wu JM, Huang HL. Microwave properties of zinc, barium and lead borosilicate glasses. *J Non-Cryst Solids* 1999**, 260**: 116-124.
[19] Tzou WC, Yang CF, Chen YC, *et al*. Improvements in the sintering and microwave properties of $BiNbO_4$ microwave ceramics by V_2O_5 addition. *J Eur Ceram Soc* 2000**, 20**: 991-996.
[20] Li EZ, Chen YW, Xiong J, *et al*. Low-temperature firing and microwave dielectric properties of Ba-Nd-Ti with composite doping Li-B-Si and Ba-Zn-B glasses. *J Mater Sci - Mater Electron* 2016**, 27**: 8428-8432.
[21] Kim MH, Lim JB, Kim JC, *et al*. Synthesis of $BaCu(B_2O_5)$ ceramics and their effect on the sintering temperature and microwave dielectric properties of $Ba(Zn_{1/3}Nb_{2/3})O_3$ ceramics. *J Am Ceram Soc* 2006**, 89**: 3124-3128.
[22] Huang CL, Weng MH, Lion CT, *et al*. Low temperature sintering and microwave dielectric properties of $Ba_2Ti_9O_{20}$ ceramics using glass additions. *Mater Res Bull* 2000**, 35**: 2445-2456.
[23] Zhou HF, Wang H, Zhou D, *et al*. Effect of ZnO and B_2O_3 on the sintering temperature and microwave dielectric properties of $LiNb_{0.6}Ti_{0.5}O_3$ ceramics. *Mater Chem Phys* 2008**, 109**: 510-514.
[24] Li EZ, Niu N, Wang J, *et al*. Effect of Li-B-Si glass on the low temperature sintering behaviors and microwave dielectric properties of the Li-modified ss-phase Li_2O-Nb_2O_5-TiO_2 ceramics. *J Mater Sci - Mater Electron* 2015**, 26**: 3330-3335.
[25] Zhou D, Pang LX, Wang DW, et *al*. High permittivity and low loss microwave dielectrics suitable for 5G resonators and low temperature co-fired ceramic architecture. *J Mater Chem C* 2017**, 5**: 10094-10098.
[26] Pang LX, Zhou D, Qi ZM, *et al*. Structure-property relationships of low sintering temperature scheelite-structured $(1-x)BiVO_{4-x}LaNbO_4$ microwave dielectric ceramics. *J Mater Chem C* 2017**, 5**: 2695-2701.
[27] Lu X, Fang B, Zhang S, *et al*. Decreasing sintering temperature for BCZT lead-free ceramics prepared via hydrothermal route. *Funct Mater Lett* 2017**, 10**.
[28] Huang CL, Wang JJ, Huang CY. Sintering behavior and microwave dielectric properties of nano alpha-alumina. *Mater Lett* 2005**, 59**: 3746-3749.
[29] Bafrooei HB, Feizpour M, Sayyadi-Shahraki A, *et al*. High-performance $ZnTiNb_2O_8$ microwave dielectric ceramics produced from $ZnNb_2O_6$-TiO_2 nano powders. *J Alloys Compd* 2020**, 834**: 9.
[30] Liu F, Liu SJ, Cui XJ, *et al*. Ordered domains and microwave properties of sub-micron structured $Ba(Zn_{1/3}Ta_{2/3})O_3$ ceramics obtained by spark plasma sintering. *Materials* 2019**, 12**: 11.

[31] Bari M, Taheri-Nassaj E. Taghipour-Armaki H. Role of nano- and micron-sized particles of TiO_2 additive on microwave dielectric properties of Li_2ZnTi_3O8-4wt% TiO_2 ceramics. *J Am Ceram Soc* 2013**, 96**: 3737-3741.
[32] Yoon SH, Choi G-K, Kim D-W, *et al*. Mixture behavior and microwave dielectric properties of $(1-x)\ CaWO_{4-x}TiO_2$. *J Eur Ceram Soc* 2007**, 27**: 3087-3091.
[33] Pan HL, Mao YX, Cheng L, *et al*. New $Li_3Ni_2NbO_6$ microwave dielectric ceramics with the orthorhombic structure for LTCC applications. *J Alloys Compd* 2017**, 723**: 667-674.
[34] Zhang P, Hao MM, Mao XR, *et al*. A novel low sintering temperature scheelite-structured $CaBiVMoO_8$ microwave dielectric ceramics. *J Alloys Compd* 2020**, 840**: 6.
[35] Ullah B, Lei W, Cao QS, *et al*. Structure and microwave dielectric behavior of A-site-doped $Sr_{(1-1.5x)}Ce_xTiO_3$ ceramics system. *J Am Ceram Soc* 2016**, 99**: 3286-3292.
[36] Lan XK, Li J, Zou ZY, *et al*. Lattice structure analysis and optimised microwave dielectric properties of $LiAl_{1-x}(Zn_{0.5}Si_{0.5})_xO_2$ solid solutions. *J Eur Ceram Soc* 2019**, 39**: 2360-2364.
[37] Ferreira VM, Baptista JL. Preparation and microwave dielectric properties of pure and doped magnesium titanate ceramics. *Mater Res Bull* 1994**, 29**: 1017-1023.
[38] Lei W, Lu WZ, Wang XC, *et al*. Effects of $CaTiO_3$ on microstructures and properties of $(1-x)\ ZnAl_2O_{4-x}Mg_2TiO_4$ (x=0.1) microwave dielectric ceramics. *Int J Inorg Mater* 2009**, 24**: 957-961.
[39] Zhang P, Zhao YG, Li LX. The correlations among bond ionicity, lattice energy and microwave dielectric properties of $(Nd_{1-x}La_x)NbO_4$ ceramics. *Phys Chem Chem Phys* 2015**, 17**: 16692-16698.
[40] Zhao YG, Zhang P. High-Q microwave dielectric ceramics using $Zn_3Nb_{1.88}Ta_{0.12}O_8$ solid solutions. *J Alloys Compd* 2016**, 662**: 455-460.

Table 1 Microwave dielectric properties and optimal sintering temperatures of $MgO\text{-}2B_2O_3\text{-}x$wt%$H_3BO_3\text{-}y$wt%BCB ceramics.

Compound	S.T. (ºC)	$Q\times f$ (GHz)	ε_r	τ_f (ppm/℃)
$MgO\text{-}2B_2O_3$-2wt%BCB-10wt%H_3BO_3	950℃/4h	36,954	4.37	-50
$MgO\text{-}2B_2O_3$-2wt%BCB-20wt%H_3BO_3	900℃/4h	33,591	4.44	-35
$MgO\text{-}2B_2O_3$-2wt%BCB-30wt%H_3BO_3	900℃/4h	37,251	4.51	-51
$MgO\text{-}2B_2O_3$-2wt%BCB-40wt%H_3BO_3	900℃/4h	35,981	4.59	-47
$MgO\text{-}2B_2O_3$-4wt%BCB-10wt%H_3BO_3	925℃/4h	40,076	4.81	-40
$MgO\text{-}2B_2O_3$-4wt%BCB-20wt%H_3BO_3	900℃/4h	42,708	5.00	-45
$MgO\text{-}2B_2O_3$-4wt%BCB-30wt%H_3BO_3	900℃/4h	43,425	5.06	-42
$MgO\text{-}2B_2O_3$-4wt%BCB-40wt%H_3BO_3	900℃/4h	44,306	5.10	-32
$MgO\text{-}2B_2O_3$-6wt%BCB-10wt%H_3BO_3	850℃/4h	37,917	5.31	-62
$MgO\text{-}2B_2O_3$-6wt%BCB-20wt%H_3BO_3	850℃/4h	40,465	5.05	-59
$MgO\text{-}2B_2O_3$-6wt%BCB-30wt%H_3BO_3	850℃/4h	41,477	5.07	-38
$MgO\text{-}2B_2O_3$-6wt%BCB-40wt%H_3BO_3	800℃/4h	37,718	5.21	-40
$MgO\text{-}2B_2O_3$-8wt%BCB-10wt%H_3BO_3	850℃/4h	38,664	5.11	-61
$MgO\text{-}2B_2O_3$-8wt%BCB-20wt%H_3BO_3	825℃/4h	33,985	5.28	-60
$MgO\text{-}2B_2O_3$-8wt%BCB-30wt%H_3BO_3	825℃/4h	34,618	5.26	-50

$MgO\text{-}2B_2O_3\text{-}8wt\%BCB\text{-}40wt\%H_3BO_3$	800℃/4h	36,064	5.12	-51

Figure Captions:

Fig.1 XRD patterns of $MgO\text{-}2B_2O_3\text{-}10wt\%H_3BO_3\text{-}y wt\%BCB$ (y = 2, 4, 6 and 8) ceramics sintered at their optimal temperatures: (a) y = 2, 950°C, (b) y = 4, 925°C, (c) y = 6, 850°C (d) y = 8, 825°C.

Fig.2 SEM images of $MgO\text{-}2B_2O_3\text{-}10wt\%H_3BO_3\text{-}y wt\%BCB$ ceramics sintered at their optimal temperatures for 4 h: (a) y = 2, 950 °C, (b) y = 4, 925 °C, (c) y = 6, 850 °C, and (d) y = 8, 825 °C

Fig.3 The variation in bulk density, ε_r, $Q\times f$ and τ_f values of $MgO\text{-}2B_2O_3\text{-}10wt\%H_3BO_3\text{-}y wt\%BCB$ (y = 2, 4, 6, and8) ceramics after sintering at different temperatures.

Fig.4 XRD patterns of the $MgO\text{-}2B_2O_3\text{-}x wt\%H_3BO_3\text{-}4wt\%BCB$ ($10 \leq x \leq 40$) ceramics sintered at different temperature: (a) x = 10, 925 °C, (b) x = 20, 900 °C, (c) x = 30, 900 °C, and (d) x = 40, 900 °C.

Fig.5 SEM images of $MgO–2B_2O_3\text{-}x wt\%H_3BO_3\text{-}4wt\%BCB$ (x = 10, 20, 30 and 40) ceramics sintered at their optimal temperatures: (a) x = 10, 925 °C, (b) x = 20, 900 °C, (c) x = 30, 900 °C, and (d) x = 40, 900 °C.

Fig.6 The bulk density, relative permittivity, $Q\times f$ and τ_f values of the $MgO\text{-}2B_2O_3\text{-}x wt\%H_3BO_3$($x$=10-40)-4wt%BCB ceramics at different sintering temperatures.

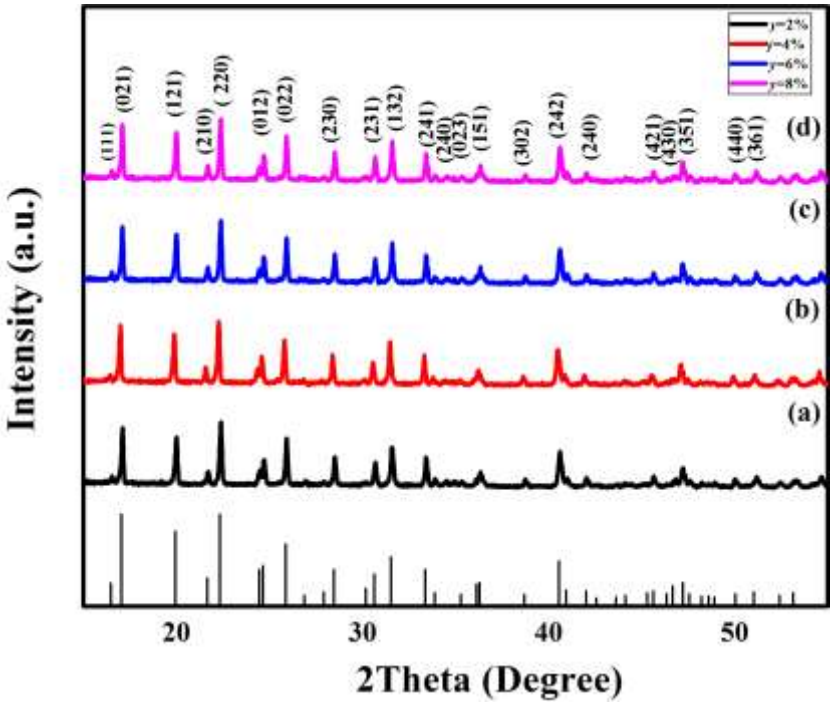
y=2%
y=4%
y=6%
y=8%
(111)
(021)
(121)
(210)
(220)
(012)
(022)
(230)
(231)
(132)
(241)
(240)
(023)
(151)
(302)
(242)
(240)
(421)
(430)
(351)
(440)
(361)
(d)
(c)
(b)
(a)
Intensity (a.u.)
20
30
40
50
2Theta (Degree)

FIG. 1

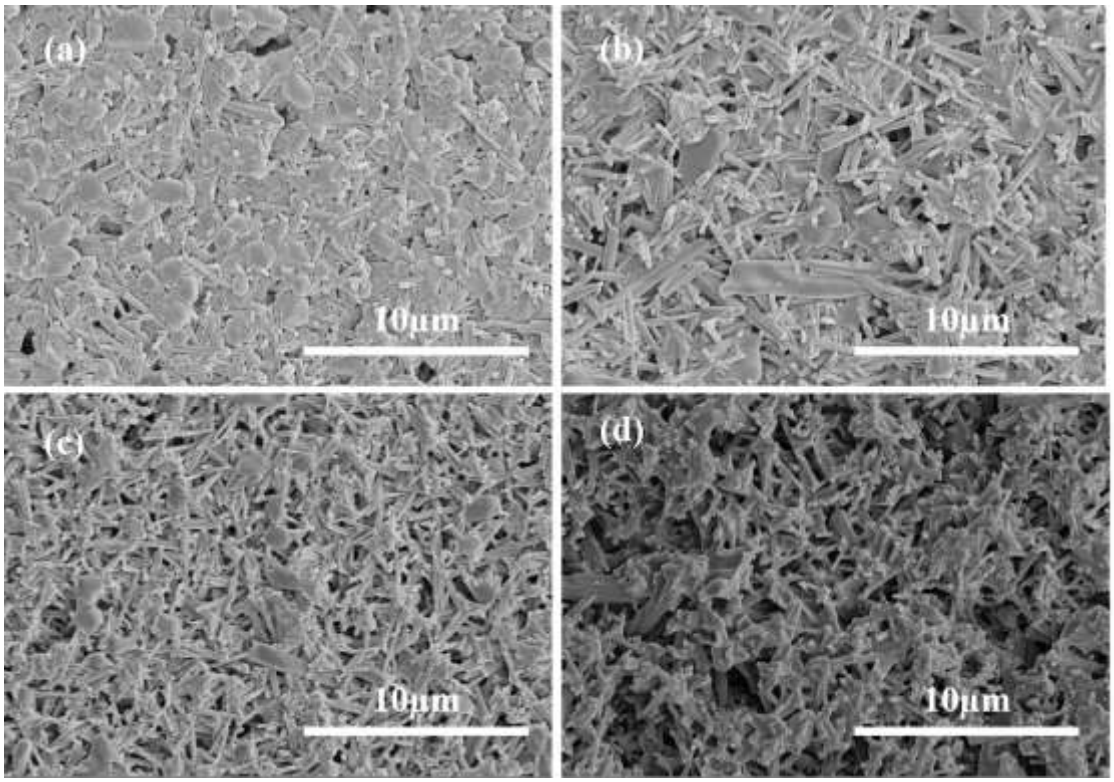

FIG. 2

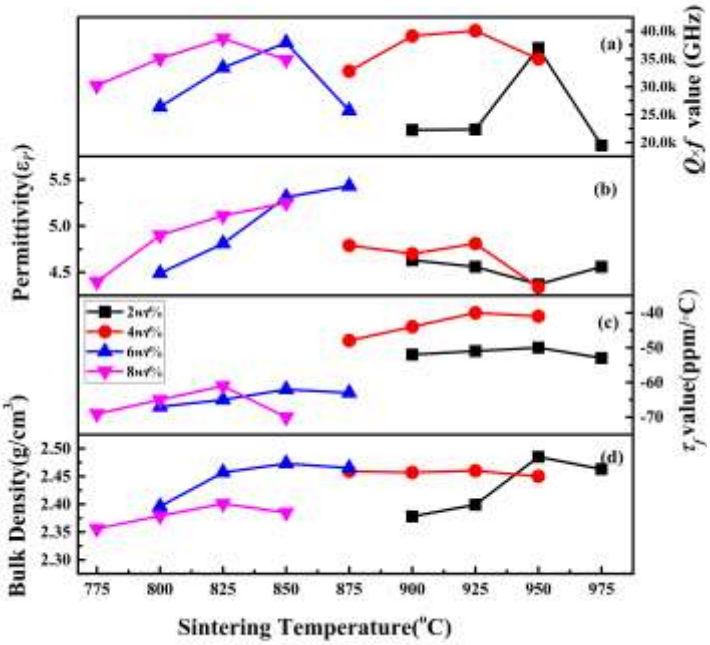
(a)
(b)
(c)
(d)
2wt%
4wt%
6wt%
8wt%
Permittivity(ε_r)
$Q\times f$ value (GHz)
τ_f value(ppm/°C)
Bulk Density(g/cm^3)
Sintering Temperature(°C)
775
800
825
850
875
900
925
950
975

FIG. 3

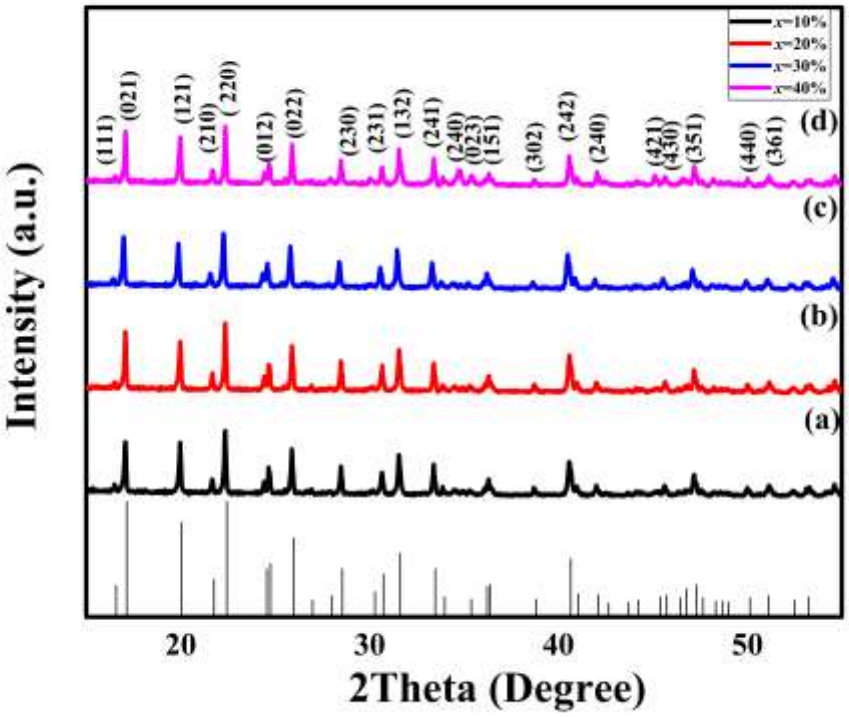
x=10%
x=20%
x=30%
x=40%
(111)
(021)
(121)
(210)
(220)
(012)
(022)
(230)
(231)
(132)
(241)
(240)
(023)
(151)
(302)
(242)
(240)
(421)
(430)
(351)
(440)
(361)
(d)
(c)
(b)
(a)
Intensity (a.u.)
20
30
40
50
2Theta (Degree)

FIG. 4

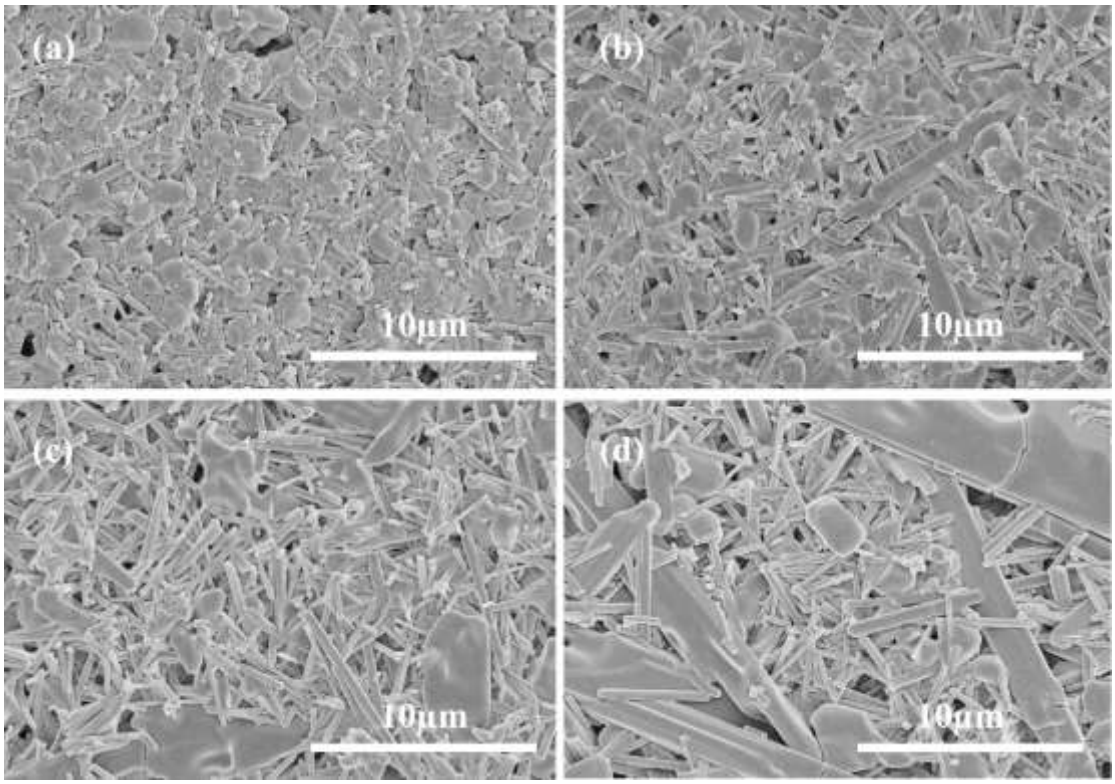

FIG. 5

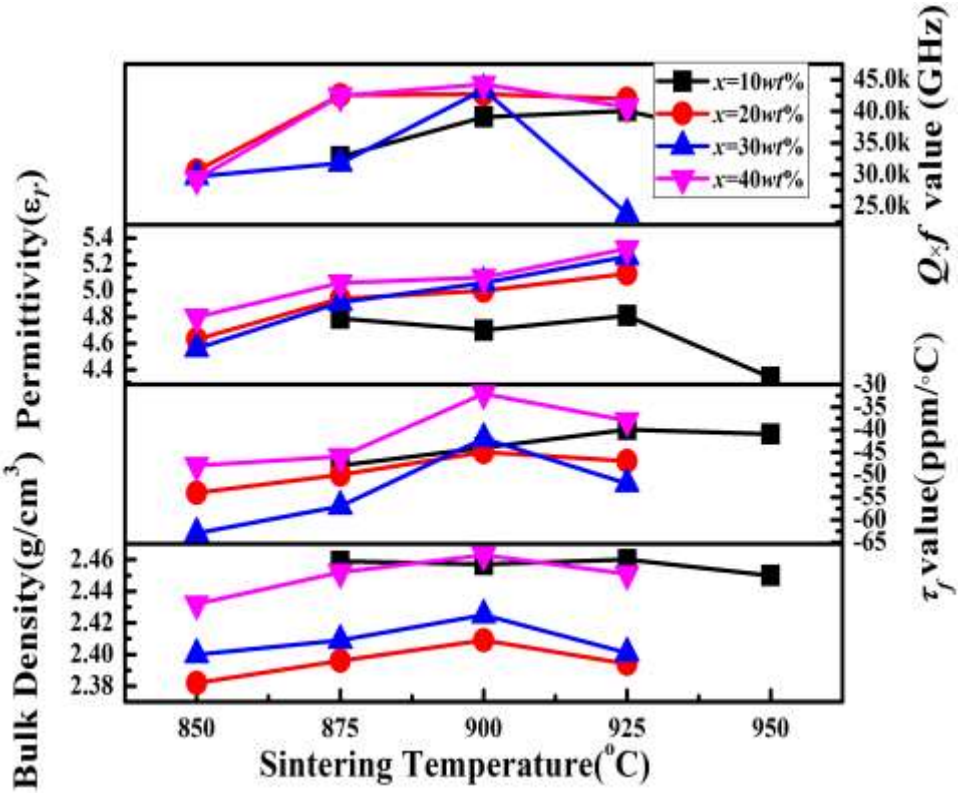
x=10wt%
x=20wt%
x=30wt%
x=40wt%
45.0k
40.0k
35.0k
30.0k
25.0k
Q×f value (GHz)
5.4
5.2
5.0
4.8
4.6
4.4
Permittivity(εr)
-30
-35
-40
-45
-50
-55
-60
-65
τf value(ppm/°C)
2.46
2.44
2.42
2.40
2.38
Bulk Density(g/cm3)
850
875
900
925
950
Sintering Temperature(°C)

FIG. 6